A Tight Junction-Associated Merlin-Angiomotin Complex Mediates Merlin's Regulation of Mitogenic Signaling and Tumor Suppressive Functions

Chunling Yi[1], **Scott Troutman**[1], **Daniela Fera**[2,3], **Anat Stemmer-Rachamimov**[4], **Jacqueline L. Avila**[1], **Neepa Christian**[1], **Nathalie Luna Persson**[5], **Akihiko Shimono**[6], **David W. Speicher**[1], **Ronen Marmorstein**[2,3], **Lars Holmgren**[5], and **Joseph L. Kissil**[1,6]

[1] Molecular and Cellular Oncogenesis Program, The Wistar Institute, Philadelphia, Pennsylvania 19104, USA

[2] Gene Expression and Regulation Program, The Wistar Institute, Philadelphia, Pennsylvania 19104, USA

[3] Department of Chemistry, University of Pennsylvania, Philadelphia, PA, 19104, USA

[4] Department of Pathology, Massachusetts General Hospital, Boston, Massachusetts 02114

[5] Department of Oncology-Pathology, Cancer Center Karolinska Institutet, SE-17176 Stockholm, Sweden

[6] Cancer Science Institute of Singapore, National University of Singapore, Singapore 117456

Summary

The Merlin/*NF2* tumor suppressor restrains cell growth and tumorigenesis by controlling contact-dependent inhibition of proliferation. We have identified a tight-junction-associated protein complex comprising Merlin, Angiomotin, Patj, and Pals1. We demonstrate that Angiomotin functions downstream of Merlin and upstream of Rich1, a small GTPase Activating Protein, as a positive regulator of Rac1. Merlin, through competitive binding to Angiomotin, releases Rich1 from the Angiomotin-inhibitory complex, allowing Rich1 to inactivate Rac1, ultimately leading to attenuation of Rac1 and Ras-MAPK pathways. Patient-derived Merlin mutants show diminished binding capacities to Angiomotin and are unable to dissociate Rich1 from Angiomotin or inhibit MAPK signaling. Depletion of Angiomotin in *Nf2*$^{-/-}$ Schwann cells attenuates the Ras-MAPK signaling pathway, impedes cellular proliferation *in vitro* and tumorigenesis *in vivo*.

Keywords

NF2; Merlin; Angiomotin; Rich1; Rac1; Tight Junction

[6]Corresponding author. jkissil@wistar.org; Phone: 1-215-898-3874.

Introduction

Neurofibromatosis Type 2 (NF2), an autosomal dominant disorder characterized by development of bilateral vestibular schwannomas, is caused by mutations and loss of heterozygosity (LOH) of the *NF2* tumor suppressor gene (Hanemann, 2008). Biallelic *NF2* inactivation also underlies various sporadic tumors of the nervous system, including almost all schwannomas, 50–60% of meningiomas and 29–38% of ependymomas (Hanemann, 2008). In corroboration of *NF2*'s inactivation as an initiating factor for these tumors, mouse models specifically deleting *Nf2* in either Schwann or arachnoidal cells develop human-like schwannomas or meningiomas, respectively (Giovannini et al., 2000; Kalamarides et al., 2002). Homozygous somatic mutations of the *NF2* gene have also been detected in malignant mesothelioma (50%), thyroid (17%), bladder (11%), skin (5%), stomach (5%), bone (3%), kidney (2%), breast (2%), and intestine (2%) cancers (http://www.sanger.ac.uk/perl/genetics/CGP/cosmic?action=gene&ln=NF2).

The *NF2* gene encodes a 69-kDa protein called Merlin (**M**oesin, **e**zrin, and **r**adixin **li**ke protei**n**) that contains an N-terminal FERM domain, followed by an α-helical domain and a charged C-terminal tail. Under growth-permissive (sparse) conditions, Merlin is phosphorylated by p21-activated kinase 1 (Pak1) or cAMP-dependent kinase A (PKA) on serine 518 within its C-terminal tail (Alfthan et al., 2004; Kissil et al., 2002; Rong et al., 2004; Xiao et al., 2002), which presumably prevents binding of the FERM domain to the C-terminal tail, leaving Merlin in an "open" and inactive conformation. Upon increased confluency and the formation of cell:cell contacts, Merlin is dephosphorylated by myosin phosphatase MYPT1–PP1δ (Jin et al., 2006), which is thought to convert Merlin to a "closed" and active state. However, several recent studies have raised questions on whether Merlin is indeed regulated by such conformational changes (Hennigan et al., 2010; Lallemand et al., 2009; Schulz et al., 2010).

As cells reach confluency, Merlin is recruited to cell junctions, where it coordinates the establishment of intercellular contacts with the concomitant inhibition of cell proliferation. The recruitment of Merlin to cell junctions is crucial for its tumor suppressive function, as patient-derived mutations that impair Merlin junctional localization render the protein inactive (Deguen et al., 1998; Lallemand et al., 2003; Stokowski and Cox, 2000).

Although the exact mechanisms by which Merlin confers contact dependent inhibition of cell growth remain unclear, it appears to involve regulation of receptor tyrosine kinases (RTKs) and downstream mitogen-activated protein kinase (MAPK) pathways. Several recent studies have illustrated that loss of Merlin leads to accumulation of RTKs at the cell surface, possibly due to defects in receptor trafficking (Ammoun et al., 2008; Lallemand et al., 2009; Maitra et al., 2006). Alternatively, Merlin has been suggested to inhibit RTKs by sequestering them to microdomains of the plasma membrane (Curto et al., 2007).

Downstream of RTKs, Merlin has been shown to inhibit Ras-mediated activation of ERK/MAPK signaling (Ammoun et al., 2008; Morrison et al., 2007). The full activation of ERK requires the phosphorylation of c-Raf (serine 338) and MEK1 (serine 298) by the p21-activated kinases (Paks), the immediate downstream effectors of Rac1 (Beeser et al., 2005). Previous work by our lab and others has shown that Merlin functions to inhibit Rac1-mediated activation of Paks (Kissil et al., 2003; Xiao et al., 2005). In addition to abnormal Pak1 activation, Merlin deficiency in NF2 patients is associated with elevated levels of Rac1-GTP, suggesting that Merlin has additional functions upstream of the Rac1-Pak axis (Kaempchen et al., 2003). Indeed, expression of dominant-active Rac1 as well as dominant-active Pak prevents Merlin from inhibiting Ras-induced activation of MAPK signaling (Morrison et al., 2007). Another study has shown that Merlin inhibits contact-dependent

recruitment of active Rac1 to the plasma membrane in endothelial cells (Okada et al., 2005). Thus, how Merlin coordinately regulates Rac1 and Ras signaling from regions of cell:cell contact remains to be defined.

Results

Merlin associates with the Angiomotin/Patj/Pals1 complex

To identify proteins that form stable complexes with Merlin, we generated human embryonic kidney (HEK293) cell lines stably expressing Flag-tagged Merlin. Affinity purification using Flag antibody-coupled beads yielded a number of protein bands that specifically co-purified with Flag-Merlin (Figure S1A). LC-MS/MS analysis identified these proteins as Angiomotin (both p80 and p130 isoforms), Angiomotin-like 1, Patj, and Pals1 (Figures S1B and S1C). Angiomotin (Amot), Angiomotin-like 1 (Amotl1, also known as JEAP), and Angiomotin-like 2 (Amotl2) form the *Motin* family. Interestingly, all members of the *Motin* family have been shown to associate with tight junctions (TJs) through binding to Patj and Pals1 (Ernkvist et al., 2009; Sugihara-Mizuno et al., 2007; Wells et al., 2006). We focused on the characterization of Merlin-Angiomotin interactions as the two Angiomotin isoforms exhibited the highest peptide match numbers in our purified Merlin-containing complexes (Figure S1C).

Merlin interacts directly with Angiomotin through their mutual coiled-coil domains

HEK293 cells endogenously express Amot-p80 and Amot-p130. We first verified that Merlin interacts with both isoforms of Angiomotin by immunoprecipitation (IP) with Flag antibodies from HEK293 cells transfected with expression vectors for Flag-Angiomotin (either Amot-p80 or Amot-p130) (Figure 1A). To map the Merlin-interacting domain within Angiomotin, we employed Amot-p80, which corresponds to the C-terminal half (amino acid 410–1084) of Amot-p130 (Figure S1B). As shown in Figures 1A, S1B and S1D, whereas truncation mutant of Angiomotin containing the coiled-coil (CC) domain (p80CC) strongly interacts with Merlin, deletion of the CC domain of Amot-p80 (p80ΔCC) abolishes its association with Merlin but not with Patj. In contrast, the Amot-p80 (p80ΔC5) mutant lacking the C-terminal PDZ binding motif (EYLI), which has previously been shown to mediate its binding to Patj (Wells et al., 2006), still interacts with Merlin while failing to bind to Patj (Figures 1A, S1B and S1D). To test whether by interacting with Merlin and Patj through two distinct domains, Angiomotin serves as a scaffold that recruits Merlin and Patj into the same complex, we co-expressed Flag-Merlin and Patj-Myc in HEK293 cells carrying control (−) or Amot shRNAs (+). As shown in Figure S1E, IP of Patj-Myc fails to pull down Flag-Merlin when Angiomotin is knocked down, suggesting that Merlin-Patj association is mediated by Angiomotin. A previous study has shown that Angiomotin complexes with Pals1 via Patj (Wells et al., 2006). Consistent with this finding, we found that Merlin requires the co-expression of both Angiomotin and Patj to co-precipitate with Pals1 (Figure S1F).

Merlin exists as two major isoforms in the cell, reported to display differential interactions with some binding partners (Ramesh, 2004). Compared to isoform 1, which was used in our purification, Merlin isoform 2 has an altered C-terminus due to alternative splicing (Ramesh, 2004). Flag-IP from HEK293 cells co-expressing Flag-Amot-p80 with HA-tagged Merlin indicated that both isoforms of Merlin interact equally well with Angiomotin (Figure 1B). Phosphorylation of Merlin at Serine 518 has been linked to its growth suppressive activity (Okada et al., 2005; Schulz et al., 2010; Shaw et al., 2001). Nonetheless, we found that both S518A (unphosphorylated) and S518D (phospho-mimicking) mutants of Merlin retain the ability to interact with Angiomotin (Figure 1B).

To map the Angiomotin-binding domain within Merlin, we expressed various HA-tagged Merlin truncation mutants (Figure 1C) along with Flag-Amot-p80 in HEK293 cells. IP with HA antibodies demonstrated that Merlin deletion mutants containing the predicted CC domains from either the α-helical region or the C-terminal domain are able to bind to Angiomotin (Figures 1C, 1D and S1G). Furthermore, several alleles of Merlin carrying patient-derived deletion or point mutations within the α-helical region exhibited diminished affinity for Angiomotin (Figure 1E). These mutations do not affect Merlin's interaction with Pak1 (Figure S1H), which we have previously shown to be mediated by the N-terminal FERM domain of Merlin (Kissil et al., 2003). Taken together, these data suggest that Merlin and Angiomotin associate through their mutual CC domains.

We next confirmed that Angiomotin specifically interacts with physiological levels of Merlin. IP with an Angiomotin antibody, but not control IgG, pulled down endogenous Merlin along with endogenous Angiomotin from wild-type HEK293 cells, while only residual amounts of Merlin and Angiomotin were precipitated in HEK293 cells expressing Angiomotin shRNAs (Figures 1F and S1I). Ezrin, another CC-domain containing ERM protein, did not co-precipitate with Angiomotin (Figure 1F), suggesting that Angiomotin selectively interacts with Merlin.

To assess the extent of Merlin-Angiomotin interaction in cells, we co-expressed Flag-Amot-p80 and Merlin tagged with both Flag and HA in HEK293 cells. Immunoblotting (IB) analysis with Flag antibody, which detects both exogenous Merlin and Amot-p80, indicated similar levels of expression for both proteins (Figure S1J, lower panel). By performing IP with HA antibody followed by IB with Flag antibody, we estimate that about 10–20% of the total Angiomotin associates with Merlin in HEK293 cells under these experimental conditions (Figure S1J, upper panel).

Finally, through *in vitro* binding assays using purified recombinant proteins, we demonstrated direct binding between Merlin and Angiomotin (Figures 1G and S4C). In attempts to estimate the *in vitro* stoichiometry of the Merlin/Angiomotin complex by gel filtration analysis, we found that free Angiomotin oligomerizes into an apparent hexamer or higher-order species, whereas Merlin exists primarily as a monomer, consistent with a recent report (Hennigan et al., 2010) (Figure S1K and data not shown). The peak of the Merlin/Angiomotin complex runs too close to the void volume to allow estimation of its molecular weight (Figure S1K).

Angiomotin retains Merlin at mature TJs in epithelial cells

Given the interaction between Merlin and Angiomotin in HEK293 cells, we examined the subcellular localization of endogenous Merlin and Angiomotin in these cells by immunofluorescence (IF). We first validated the specificity of Merlin and Angiomotin antibodies using Merlin- or Angiomotin- knockdown (KD) or knockout (KO) cells. As shown in Figures S2A-S2C, both antibodies stained along cell boundaries in wild type HEK293 or primary mouse kidney (BMK) cells, and the respective signals were dramatically reduced or completely eliminated in Merlin- or Angiomotin- KD/KO cells. Furthermore, endogenous Merlin and Angiomotin co-localize with the TJ marker ZO1 and with each other in HEK293 cells (Figure 2A), consistent with the two proteins forming a complex at the TJs.

Merlin has been previously shown to localize to AJs in mouse embryonic fibroblasts and keratinocytes (Lallemand et al., 2003). The co-localization of Merlin with Angiomotin and ZO1 in HEK293 cells suggests that Merlin also localizes to TJs. Since HEK293 cells do not form mature belt-like junctional structures, we switched to MDCK cells to further characterize Merlin and Angiomotin localization. Co-staining of endogenous Merlin with

either E-Cadherin (an AJ marker) or ZO1 (a TJ marker) and subsequent confocal Z-stack analysis along the apical-basolateral axis revealed that Merlin partially co-localized with both AJ and TJ markers in MDCK cells (Figures 2B and 2C). Similarly, Angiomotin localization has been shown to overlap with both AJ and TJ markers in MDCK cells (Wells et al., 2006).

To study its recruitment kinetics to cell junctions, the localization of Merlin was examined following a calcium switch. Briefly, after overnight incubation in Low Calcium Medium (LCM), cells were switched back to High Calcium Medium (HCM) and fixed at different time points. We have previously shown that both Angiomotin isoforms were recruited to the junctions several hours after switching to HCM in MDCK cells (Ernkvist et al., 2008). In contrast, Merlin regained junctional localization as early as 15 minutes after the switch, similar to ZO1 (Figure S2D). At this point in time, only primordial junctional structures would have been formed (Miyoshi and Takai, 2005). This early recruitment of Merlin to the primordial junctions is likely mediated by E-Cadherin or β-Catenin, proteins that have been shown to interact with Merlin (Curto et al., 2007; Lallemand et al., 2003).

Although Angiomotin does not appear to participate in the initial recruitment of Merlin to primordial junctions, it may control the subsequent redistribution of a portion of Merlin to mature TJs. To address this possibility, we transfected MDCK cells with Flag-tagged Angiomotin p80, p130, or p80ΔC5. As shown in Figure 2D, cells overexpressing Angiomotin p80 or p130 exhibited increased localization of endogenous Merlin to TJs, compared to neighboring untransfected cells. In contrast, overexpression of p80ΔC5 without the TJ-tethering domain resulted in a significant shift of Merlin from cell junctions to peri-junctional regions in the cytoplasm (Figure 2D). As a control, we transfected MDCK cells with Flag-p80ΔCC, which is localized throughout the cytoplasm, but not to the cell junctions (Figure S2E). Consistent with our finding that p80ΔCC does not interact with Merlin (Figures 1A and S1D), the distribution of Merlin in p80ΔCC-transfected cells was essentially indistinguishable from surrounding untransfected cells (Figure S2E). Taken together, these data suggest that while the recruitment of Merlin to early junctional structures likely does not involve Angiomotin, the retention of Merlin at mature TJs is mediated by Angiomotin.

Angiomotin functions downstream of Merlin and upstream of Rich1 as a positive regulator of Rac1 and MAPK signaling

A similar TJ-associated protein complex containing Angiomotin, Patj and Pals1 has previously been purified from HEK293 cells using a RhoGAP domain containing protein, Rich1 (also known as ARHGAP17 or Nadrin), as bait (Wells et al., 2006). In this report, the authors showed that Rich1 functions as a Cdc42 GAP and that Angiomotin, through direct interaction with Rich1, negatively regulates the GAP activity of Rich1. Two other studies reported that Rich1 is also active towards Rac1 (Harada et al., 2000; Richnau and Aspenstrom, 2001). To determine the activity of Rich1 in HEK293 cells, we used siRNAs to knockdown endogenous Rich1 expression and examined endogenous Rac1-GTP and Cdc42-GTP levels. As shown in Figure S3A, depletion of Rich1 in HEK293 cells increased the endogenous levels of active Rac1 without affecting Cdc42 activity. In contrast, Angiomotin knockdown (Amot-KD) HEK293 cells exhibited a decrease in endogenous Rac1-GTP, while levels of active Cdc42 remained unchanged (Figures 3A and S3B). These results suggest that Rich1 and Angiomotin regulate Rac1-GTP levels in HEK293 cells, but do not exclude the possibility that they may also modulate Cdc42-GTP levels in other cell types, as shown by other studies (Harada et al., 2000; Wells et al., 2006).

Merlin has been previously shown to function as a negative regulator of Rac1, through which it inhibits the phosphorylation/activation of Ras-MAPK signaling effectors such as c-

Raf, MEK1/2 and ERK (Ammoun et al., 2008; Morrison et al., 2007). Based on our finding that Angiomotin and Rich1 also modulate Rac1 activity (Figures 3A S3A, and S3B), we focused on how Merlin, Angiomotin and Rich1 may function together to regulate Rac1 and Ras-MAPK signaling.

To determine whether Angiomotin indeed plays a role in regulating MAPK signaling, we introduced two independent shRNAs targeting both isoforms of Angiomotin either separately or in combination (Amotsh #1, #2, or #1+#2) into HEK293 cells and found that both shRNAs reduced the levels of endogenous Angiomotin and led to a decrease in pERK (T202/204) levels, which was rescued by the re-introduction of either Angiomotin isoform (Figures S3C and S3D). As combination of the two shRNAs resulted in an almost complete depletion of endogenous Angiomotin, we established two independent HEK293 lines (Amot-KD #2 and #8) stably expressing both Amot shRNAs and carried out subsequent studies with these two clones. In addition to lowering the levels of Rac1-GTP, silencing of Angiomotin led to decreased phosphorylation of c-Raf (S338), MEK (S298), ERK (T202/204), p95RSK (S380) and BAD (S112), all of which are phosphorylation sites associated with an activated state of the MAPK pathway (Figures 3A, 3F, and S3E). In contrast, the phosphorylation of BAD (S136), a phosphorylation event downstream of PI3K-AKT signaling, was unaffected by Angiomotin diminution (Figure S3E). These data indicate that Angiomotin regulates the Rac1-Pak axis and downstream MAPK signaling in an opposite manner from Merlin and Rich1.

To establish the hierarchy of Merlin, Angiomotin and Rich1 in controlling Rac1 and MAPK signaling, we introduced a "smartpool" or deconvoluted siRNAs targeting Merlin and/or Rich1 into control or Amot-KD HEK293 cells and assessed Rac1 activity and MAPK signaling in these cells. Consistent with Merlin and Rich1 acting as negative regulators, knockdown of either endogenous Merlin or endogenous Rich1 in wild type HEK293 cells elevated the levels of active Rac1, phospho-MEK and phospho-ERK (Figures 3B, S3F, and S3G). Notably, simultaneous depletion of Merlin and Rich1 did not further enhance Rac1 activity and downstream MAPK signaling (Figure 3B), suggesting that the two proteins function within a linear pathway. In Amot-KD HEK293 cells, while silencing of Merlin failed to reverse the down-regulation of Rac1-GTP levels and MAPK signaling caused by the loss of Angiomotin, elimination of Rich1 restored the levels of Rac1-GTP and MEK/ERK phosphorylation to near those of control cells (Figure 3B), thus placing Angiomotin downstream of Merlin and upstream of Rich1 in modulating Rac1 activation and Ras-MAPK signaling (Figure 3F).

To assess whether Rich1 indeed mediates Merlin's regulation of Rac1 and the MAPK pathway, we co-transfected Flag-Merlin with either a non-silencing control or Rich1 siRNAs into HEK293 cells. As shown in Figure 3C, overexpression of Flag-Merlin reduced the levels of active Rac1 and phosphorylated c-Raf and ERK in cells co-transfected with control siRNAs, but not in cells co-expressing Rich1 siRNAs. Therefore, Merlin requires Rich1 to inhibit Rac1 and MAPK signaling.

Finally, we confirmed that Angiomotin and Rich1 function through the Paks to regulate the MAPK pathway. As shown in Figures 3D and 3E, expression of Pak-specific siRNAs or a constitutive active form of Pak (CA-Pak3) eliminated the effects of Rich1 or Amot knockdowns on MAPK signaling, respectively.

Merlin negatively regulates Rac1 activity and MAPK signaling by competing with Rich1 for Angiomotin binding

Our data so far have established a regulatory pathway upstream of Rac1, in which Merlin, Angiomotin and Rich1 function as upstream inhibitors of each other (Figure 3F).

Considering that Angiomotin interacts with Merlin through its CC domain (Figure 1A), which also mediates Angiomotin-Rich1 binding (Wells et al., 2006), we hypothesized that Merlin might function as an activator of Rich1 by dissociating it from its inhibitor Angiomotin. To test this hypothesis, we transfected HEK293 cells with Myc-Rich1, HA-Merlin and Flag-Amot-p80 and carried out IP with either Myc, HA or Flag antibodies. As shown in Figure 4A, Flag-Amot-p80 co-precipitated with both HA-Merlin and Myc-Rich1, thus corroborating that Angiomotin interacts with both Merlin and Rich1. In contrast, HA-Merlin and Myc-Rich1 did not co-precipitate, indicating that Merlin and Rich1 form distinctive complexes with Angiomotin. Similarly, *in vitro* binding assays employing purified recombinant proteins showed that Merlin and Rich1, while not interacting with each other, both directly bind to Angiomotin (Figures 1F, S4C and S4D).

To examine whether Merlin and Rich1 compete for interaction with Angiomotin, HA-Merlin and Myc-Rich1 expression vectors were introduced into HEK293 cells either separately or together, and endogenous Angiomotin was precipitated from these cells and probed with Angiomotin, HA and Myc antibodies. Whereas a similar amount of HA-Merlin was present in Angiomotin precipitates from cells expressing HA-Merlin alone or in combination with Myc-Rich1, the amount of Myc-Rich1 co-precipitated with Angiomotin was drastically diminished when HA-Merlin was co-expressed (Figure 4B), suggesting that Merlin competes with Rich1 for binding to Angiomotin.

To further assess how Merlin competes with Rich1 for Angiomotin binding, we expressed Merlin at increasing levels and analyzed Rich1-Angiomotin interactions in HEK293 cells. We found that Merlin reduces Rich1-Angiomotin association and MAPK signaling in a dose-dependent manner (Figure 4C). Similarly, addition of increasing amount of recombinant Merlin protein gradually titrates Angiomotin off Rich1 *in vitro* (Figure S4D). Importantly, tumor-derived Merlin mutants that are defective in Angiomotin binding fail to displace Rich1 from Angiomotin (Figures 1E and 4D), suggesting that the interplay between Merlin, Angiomotin and Rich1 mediates, at least in part, the tumor suppressive function of Merlin.

Based on the NCBI gene database, Rich1 is expressed as at least five splice isoforms in mouse, whereas in human only two Rich1 splice isoforms have been reported to date. In light of a previous account suggesting that different Rich1 isoforms may have distinct functions and tissue distributions (Furuta et al., 2002), we evaluated whether Merlin and Angiomotin may differentially regulate the two major isoforms of human Rich1. As shown in Figure S4A, we found no significant distinction between the two Angiomotin isoforms in terms of their binding affinities for Rich1. Likewise, both isoforms of Rich1 interact similarly with endogenous Angiomotin (Figure S4B). Nevertheless, co-expression of Merlin reduced the binding of Rich1 isoform 2 to Angiomotin to a larger extent than Rich1 isoform 1 (Figure S4B).

In search of physiological signals that might modulate the interaction of Angiomotin with Merlin and/or Rich1, we transfected HEK293 cells with Flag-Merlin and Myc-Rich1 and compared the amount of Merlin and Rich1 co-precipitated with endogenous Angiomotin under various growth conditions. Since Angiomotin co-localizes with both Merlin and Rich1 at the site of cell junctions (Figure 2A) (Wells et al., 2006), we assessed whether cell-cell contacts are required for Angiomotin to interact with either protein. Not surprisingly, in comparison to confluent cultures (C), sparsely grown cells (Sp) or cells grown in suspension (Su) show reduced interactions between both Angiomotin-Merlin and Angiomotin-Rich1 (Figure 4E), corroborating that establishment of cell junctions facilitates the assembly of Angiomotin-Merlin and Angiomotin-Rich1 complexes. Under confluent conditions that allow the formation of junctional structures, we found that serum starvation followed by

brief exposure to serum (St) dissociates Merlin from Angiomotin, while increasing the amount of Angiomotin-bound Rich1 and corresponding pMEK (S298) levels (Figure 4E). These data indicate that Angiomotin interacts dynamically with Merlin or Rich1 in response to cues from the extracellular environment, although the molecular mechanisms underlying these changes remain to be elucidated. Finally, the high level of MAPK signaling under sparse conditions, which disrupt Angiomotin-Merlin and Angiomotin-Rich1 complexes (Figure 4E), underscores the spatial and temporal constraints under which the Merlin-Angiomotin-Rich1 signal cascade operates and the existence of additional regulatory mechanisms on Rac1 activity and MAPK signaling under certain physiological conditions.

Angiomotin and Merlin interact in Schwann cells and co-localize to paranodes and Schmidt-Lantermann incisures in the myelinating peripheral nerve

Patients with mutations in the *NF2* gene develop primarily Schwann cell tumors of peripheral nerves. Thus, to ascertain the potential relevance of the Merlin-Angiomotin interaction to the tumor suppressive functions of Merlin, we first confirmed that Angiomotin, similar to Merlin, is expressed in Schwann cells (rat R3 Schwann cells, rat RT4 schwannoma cells and human MPNST 90-8TL cells) and human peripheral nerve tissue (Figures S4E and S4F).

To investigate whether Merlin and Angiomotin interact in Schwann cells, we carried out IP using Merlin or Angiomotin antibodies in RT4-67 schwannoma cells that carry a Doxycycline inducible allele of Merlin. In the absence of Doxycycline, endogenous Merlin and Angiomotin readily co-precipitated with one another (Figure 5A). Upon treatment with Doxycycline, increase in Merlin expression led to a corresponding increase in the amount of Angiomotin or Merlin co-precipitated with one another, but not with control IgGs (Figure 5A). Likewise, endogenous Merlin-Angiomotin interactions are also detectable in rat R3 and human 90-8TL cells (Figure S4F).

To examine the distribution of Angiomotin and Merlin along the highly polarized myelinating Schwann cells *in vivo*, we dissected sciatic nerve fibers from wild-type mice and stained them with Angiomotin, Merlin, and E-Cadherin antibodies. As shown in Figure 5B, both Angiomotin and Merlin co-localize with E-Cadherin to the paranodes and Schmidt-Lantermann incisures along the sciatic nerves. Thus, Merlin and Angiomotin interact and co-localize in myelinating Schwann cells, the cell type of origin for NF2-associated schwannomas.

Consistent with the hypothesis that Merlin-Angiomotin interaction is necessary for Merlin to suppress Ras-MAPK signaling, we found that patient-derived Merlin mutants defective in Angiomotin-binding (Figure 1E) also lose the capacity to inhibit c-Raf and ERK phosphorylation in RT4-67 cells (Figure 5C). As in HEK293 cells (Figure 4C), Doxycycline-induced expression of Merlin in RT4-67 cells leads to a gradual decrease in Angiomotin/Rich1 association (Figure 5D). Furthermore, formation of cell:cell contacts in RT4-67 cells are also required for the assembly of the Angiomotin/Merlin complex, which is disrupted upon serum stimulation (St), leading to an increase in Angiomotin/Rich1 association (Figure 5E). These results indicate that Merlin operates through Angiomotin and Rich1 to inhibit MAPK signaling in Schwann cells.

Depletion of Angiomotin impedes the proliferation and tumorigenic capacity of Nf2-deficient Schwann cells

The findings that Merlin and Angiomotin interact and co-localize in Schwann cells and that Merlin functions through Angiomotin to regulate growth factor mediated signaling (Figure

5) strongly suggest that deregulation of Angiomotin in *NF2*-deficient Schwann cells may contribute to tumor development caused by the loss of *NF2*.

To investigate whether Angiomotin is required for tumor development *in vivo*, we employed a mouse model of NF2 in which conditional deletion of *Nf2* in mouse Schwann cells (*P0-Cre:Nf2$^{flox/flox}$*) leads to schwannoma development, within a lag time of several months (Giovannini et al., 2000). To assess the requirement for Angiomotin in this model, we crossed the *P0-Cre* and *P0-Cre:Nf2$^{flox/flox}$* to *Amot$^{flox/flox}$* mice. While *P0-Cre:Amot$^{flox/flox}$* mice are born at the expected Mendelian ratios and develop normally, the *P0-Cre:Nf2$^{flox/flox}$:Amot$^{flox/flox}$* mice die shortly after birth due to neurological defects (Yi and Kissil, unpublished results), precluding the use of this model.

We therefore employed instead an orthotopic mouse model in which Schwann cells are injected intraneurally into the mouse sciatic nerve (Wong et al., 2010). First, we introduced two independent constructs expressing Angiomotin shRNAs into *Nf2*-null Schwann cells (SC4) that were derived from the sciatic nerves of *Nf2$^{flox/flox}$* mice and treated with Adeno-Cre *in vitro* to delete the *Nf2* gene (Lallemand et al., 2009). As shown in Figure S5A, a significant reduction in Angiomotin protein levels was observed in cells expressing either of the two shRNAs (sh-Amot #1 and #2). This was accompanied by a dramatic decrease in levels of phospho-MEK and phospho-ERK and led to approximately a 2-fold reduction in the growth rate of the Amot-KD SC4 cells (Figure S5B). This apparent decrease in growth rate is not due to secondary effects caused by reduced attachment or cell viability, as we observed no evidence of cell detachment (data not shown) or apoptosis in Amot-KD SC4 cells (Figure S5C). Previous studies have shown that loss of Merlin increases cell proliferation by promoting G1 to S phase progression (Okada et al., 2005; Xiao et al., 2005). To examine whether Angiomotin silencing slows the proliferation of SC4 cells by overriding the effect of *Nf2* deficiency on cell cycle progression, we carried out a BrdU incorporation assay to compare the abilities of an G0-synchronized control and Amot-KD SC4 cells to progress through G1 phase and into S phase in response to mitogenic cues. As shown in Figures 6A-6C, depleting Amot from *Nf2* null SC4 cells, similar to Merlin reconstitution, resulted in reduced BrdU incorporation rate and ERK phosphorylation, comparing to control SC4 cells. Furthermore, ablation of Angiomotin from SC4 cells with restored Merlin expression did not further lower the BrdU incorporation rate (Figures 6A and 6B), suggesting that inactivation of Angiomotin specifically inhibits the proliferation of *Nf2* deficient SC4 cells.

Next, to examine whether Angiomotin is required for tumor development driven by *Nf2* deficiency, control and Amot-KD SC4 cells carrying a luciferase reporter allele were injected intraneurally into the sciatic nerve sheaths of NOD/SCID mice, and tumor development was monitored through bioluminescence imaging (BLI). As shown in Figures 6D and 6E, one-week post surgery, substantial tumor growth was detectable in mice transplanted with control SC4 cells. In comparison, at this time point, tumor development was minimal for either of the Amot-KD lines. We also carried out an extended time course study and found that tumors from Amot-KD SC4 cells continued to grow at a significantly slower rate than those from control SC4 cells up to three weeks post surgery, at which time mice injected with control SC4 cells had to be sacrificed (Figure S5D). We analyzed three tumors from each of the control and two Amot-KD groups by western blot analysis and found that with the one exception, the majority of Amot-KD tumors maintained low levels of Amot and MAPK signaling, consistent with their slower growth rate (Figure S5E). To characterize how the orthotopic tumors invade normal sciatic nerves, we performed immunohistochemistry (IHC) with neuronal marker Tuj-1 that stains only normal nerves, and schwann cell marker p75NTR, which marks both tumor and host nerve tissues. As shown in Figure S5F, tumors derived from control SC4 cells only contain remnants of nerve

structures, which are positive for p75NTR but negative for Tuj-1. In contrast, a number of mostly intact nerve bundles positive for both p75NTR and Tuj-1 were scattered across the Amot-KD tumors, suggesting that Amot-KD results in a less aggressive tumor phenotype. Similar effects of Amot-KD on tumor growth rates were observed in a xenograft study in which control and Amot-KD SC4 cells were subcutaneously injected side by side into the flanks of NOD-SCID mice (Figures S5G and S5H).

Taken together, these data demonstrate that Angiomotin is required for schwannoma development due to loss of *Nf2* and warrant further testing of Angiomotin as a potential therapeutic target in *NF2*-driven schwannomas.

Discussion

The antagonizing Angiomotin/Merlin and Angiomotin/Rich1 signaling complexes link TJs to regulation of growth factor signaling

In addition to its well-characterized role as a permeability barrier, the TJs, mostly through the so-called "TJ cytoplasmic plaque", also serve as a platform that integrates multiple signal transduction pathways regulating cytoskeleton organization, cell polarity, cell proliferation and cell differentiation (Iden and Collard, 2008).

It is well established that the formation of junctional structures upon cell:cell contacts is pivotal to the concomitant suppression of mitogenic signaling. Disruption of TJs leads to uncontrolled cell proliferation and represents an early and key aspect in cancer metastasis, although the exact mechanisms are unclear (Forster, 2008). In this study, we have identified a TJ-associated signaling complex, in which Merlin is connected to the junctional proteins Patj and Pals1 via Angiomotin (Figure S1). Intriguingly, we find that this Merlin-containing junctional complex negatively regulates another TJ-associated Rich1/Angiomotin/Patj/Pals1 complex in response to environmental signals (Figures 4 and 5). Taken together with our other finding that Merlin, Angiomotin and Rich1 function to regulate Rac1 activity and MAPK signaling in a hierarchical manner (Figure 3), we propose the following working model: under growth suppressive conditions such as the maturation of cell junctions, Merlin releases Rich1 from Angiomotin, allowing Rich1 to inhibit Rac1 activity by converting Rac1-GTP to Rac1-GDP (Figure 7, left panel). In response to growth stimuli, Merlin becomes dissociated from Angiomotin through a yet unidentified mechanism. Unoccupied Angiomotin sequesters Rich1 at TJs, leading to an increase in Rac1 activity (Figure 7, right panel). Our finding that by forming competitive complexes with Angiomotin at the TJ cytoplasmic plaque, Merlin and Rich1 inhibit Rac1 and the Ras-MAPK mitogenic pathways provides initial clues as to how TJs might coordinately regulate multiple cellular processes such as establishment of cell polarity and suppression of cell proliferation.

The Multi-faceted Merlin Signaling Network

We and others have previously shown that Merlin can inhibit Rac1 signaling by interfering with the activation of the Paks by Rac1 (Hirokawa et al., 2004; Kissil et al., 2003; Xiao et al., 2005). In a negative feedback loop, the Paks in turn phosphorylate and inactivate Merlin (Kissil et al., 2002; Xiao et al., 2002). Additionally, it has been shown that Merlin mediates contact-dependent inhibition of cell proliferation by acting upstream of Rac1 and MAPK signaling, although the exact mechanism of how Merlin controls Rac1 activity was not defined (Morrison et al., 2007; Okada et al., 2005). The TJ-associated Merlin-Angiomotin-Rich1-Rac1-Pak signaling cascade delineated by our study provides a mechanism to explain Merlin's regulation of Rac1 (Figure 7). Notably, our current study yet again points towards the Rac1-Pak axis as a critical mediator of Merlin signaling and is consistent with our

previous work demonstrating that inhibition of Pak can counter the tumorigenic effect of Merlin inactivation (Yi et al., 2008).

In addition to inhibiting the Rac1-Pak axis, Merlin's tumor suppressive activity has been linked to growth factor receptor signaling and the Hippo/Yap pathway (Benhamouche et al., 2010; Yi and Kissil, 2010; Zhang et al., 2010). Furthermore, a recent study has showed that Merlin has additional nuclear function in inhibiting the CRL4[DCAF1] E3 ubiquitin ligase, which is also important for Merlin's tumor suppressive activity (Li et al., 2010). Therefore, the emerging picture of Merlin's tumor suppressive function is one of significant complexity. Considering that Pak, EGFR, DCAF1 and now Angiomotin have been all shown to be required for the tumor suppressive function of Merlin, it is likely that these seemingly parallel pathways are in fact inter-dependent of each other and further efforts to elucidate the relationships between these pathways will greatly facilitate the understanding of Merlin's tumor suppressive function.

We find that in contrast to Pak and DCAF1, which bind to the N-terminal FERM domain of Merlin, Angiomotin interacts with Merlin through its C-terminal CC domains (Figures 1C–1E). Also unlike DCAF1, the Merlin-Angiomotin interaction does not appear to be affected by S518 phosphorylation (Figure 1B). Nonetheless, phosphorylation could still potentially play a role in modulating Merlin-Angiomotin interaction, as additional Merlin phosphorylation sites have been described previously (Kissil et al., 2002; Shaw et al., 2001). Notably, we observed a slower migrating (presumably hyperphosphorylated) form of the Merlin S518D mutant that did not co-precipitate with Angiomotin (Figure 1B). This is consistent with a scenario in which phosphorylation at S518 primes Merlin for further posttranslational modification(s), which in turn block(s) Merlin's binding to Angiomotin. Clearly, further studies are necessary to investigate this and other potential mechanism(s) that control(s) Merlin's ability to interact with Angiomotin.

Our findings that the CC domains of Merlin from both the α-helical and C-terminal regions can mediate its binding to Angiomotin (Figures 1C, 1D and S1G) and that tumor-derived mutations within the α-helical region abate Merlin-Angiomotin interactions without affecting Merlin's ability to interact with Pak (Figures 1E and S1H) underscore a previously underappreciated role of the CC domains in mediating Merlin's tumor suppressive function and are consistent with the fact that patient-derived missense mutations are spread throughout all domains of the *NF2* gene (http://www.sanger.ac.uk/perl/genetics/CGP/cosmic?action=gene&ln=NF2).

Angiomotin – a potential player in NF2 and other Merlin-related cancers

In this study, we demonstrate that Angiomotin functions as a positive regulator of the MAPK signaling pathway (Figure 3) and is required for schwannoma development from *Nf2*-deficient Schwann cells (Figure 6). Beside schwannomas, *NF2* germline and/or somatic mutations predispose patients to meningiomas and ependymomas. Homozygous *NF2* mutations have been also detected in carcinomas of various tissue origins. In particular, a recent systematic analysis has indicated that *NF2* mutations define a subtype of non-VHL mutated clear cell renal carcinomas (ccRCCs) and targeted deletion of *Nf2* in mouse renal epithelia leads to invasive carcinoma by 6–10 months of age (Dalgliesh et al., 2010;Morris and McClatchey, 2009). In addition, *Nf2*-driven liver cancer models have been recently reported (Benhamouche et al., 2010;Zhang et al., 2010). Considering our finding that the Angiomotin-Merlin interaction mediates Merlin's regulation of Rac1-MAPK signaling in epithelial cells (Figure 3), it would be of interest to examine the role of Angiomotin in these two cancer models and the status of Angiomotin in human kidney and liver cancers.

Experimental Procedures

Anti-Angiomotin and Rich1 Antibodies

Purified rabbit polyclonal Angiomotin and Rich1 antibodies were raised against peptide sequences CKTPIQILGQEPDAEMVEYLI and GRAEKTEVLSEDLLQIERR (Thermo Scientific Open Biosystems). Specificity of antibodies was verified with Angiomotin or Rich1 knockdown cells by IP, IB and IF (Figures 1F, 3A, 3B, S1I, S2B and S2C).

Immunofluorescence

HEK293 or MDCK cells grown on coverslips were washed 3X with cold PBS and fixed by cold methanol for 5′ or by 4% paraformaldehyde for 30′. Coverslips were blocked in 5% goat serum/PBS and 0.3% Triton X-100. Teased nerve fibers were permeabilized in acetone for 10′, washed in PBS, blocked for 60′ in 5% sh skin gelatin/PBS and 0.5% Triton X-100. For co-staining with ZO1 (1:200), E-Cad (1:500) and Flag (1:500) mouse antibodies, endogenous Merlin was detected with rabbit anti-Merlin (#9168 at 1:50). For co-staining with Amot (1:200), mouse anti-Merlin (b-12 at 1:50) was used. This was followed by incubation with Fluor 488 and 568 conjugated anti-mouse or rabbit secondary antibodies at 1:400 (Invitrogen). DAPI (Sigma) was used for nuclear counterstaining. Images were taken under Zeiss Axioskop 2 fluorescence microscope or Leica TCS SP2 scanning confocal microscope. Z-stacking images were deconvoluted using Leica confocal software.

Isolation of mouse sciatic nerve

Three to four month-old mice were euthanized by CO_2 and sciatic nerves were surgically removed, xed in 4% paraformaldehyde for 10′ and rinsed in PBS. Nerves were cut into 1–2cm pieces, teased into small bundles or single bers and spread onto glass slides. Slides were allowed to dry overnight at RT and stored at −20°C.

In Vivo Tumor Models and Imaging

All animal experiments were approved by the Wistar Institutional Animal Care and Use Committee and performed in accordance with relevant institutional and national guidelines.

$Nf2^{-/-}$ SC4 control or Amot-KD Schwann cells were transduced by lentiviruses carrying pLuc-mCherry and sorted by FACS. 2×10^5 or 5×10^4 cells were transplanted into the sciatic nerve sheath of NOD/SCID mice (6–8 weeks of age) by intraneural injection or injected subcutaneously. Tumor progression was monitored weekly by bioluminescence imaging (BLI) according to the manufacturer's instructions on an IVIS-200 system (Xenogen, San Francisco, CA).

Statistical Analysis

All data were represented by the mean and standard deviation (SD) was used to indicate data variability. All statistical analysis was performed with two-tailed unpaired *Student*'s t-test.

Supplementary Material

Refer to Web version on PubMed Central for supplementary material.

Acknowledgments

Abbreviations

Amot	Angiomotin
NF2	Neurofibromatosis Type 2
TJs	Tight Junctions
AJs	Adherens Junctions
GAP	GTPase Activating Protein
RTKs	Receptor Tyrosine Kinases
MAPK	Mitogen-Activated Protein Kinase

References

Alfthan K, Heiska L, Gronholm M, Renkema GH, Carpen O. Cyclic AMP-dependent protein kinase phosphorylates merlin at serine 518 independently of p21-activated kinase and promotes merlin-ezrin heterodimerization. J Biol Chem. 2004; 279:18559–18566. [PubMed: 14981079]

Ammoun S, Flaiz C, Ristic N, Schuldt J, Hanemann CO. Dissecting and targeting the growth factor-dependent and growth factor-independent extracellular signal-regulated kinase pathway in human schwannoma. Cancer Res. 2008; 68:5236–5245. [PubMed: 18593924]

Beeser A, Jaffer ZM, Hofmann C, Chernoff J. Role of group A p21-activated kinases in activation of extracellular-regulated kinase by growth factors. J Biol Chem. 2005; 280:36609–36615. [PubMed: 16129686]

Benhamouche S, Curto M, Saotome I, Gladden AB, Liu CH, Giovannini M, McClatchey AI. Nf2/Merlin controls progenitor homeostasis and tumorigenesis in the liver. Genes Dev. 2010; 24:1718–1730. [PubMed: 20675406]

Curto M, Cole BK, Lallemand D, Liu CH, McClatchey AI. Contact-dependent inhibition of EGFR signaling by Nf2/Merlin. J Cell Biol. 2007; 177:893–903. [PubMed: 17548515]

Dalgliesh GL, Furge K, Greenman C, Chen L, Bignell G, Butler A, Davies H, Edkins S, Hardy C, Latimer C, et al. Systematic sequencing of renal carcinoma reveals inactivation of histone modifying genes. Nature. 2010; 463:360–363. [PubMed: 20054297]

Deguen B, Goutebroze L, Giovannini M, Boisson C, van der Neut R, Jaurand MC, Thomas G. Heterogeneity of mesothelioma cell lines as defined by altered genomic structure and expression of the NF2 gene. Int J Cancer. 1998; 77:554–560. [PubMed: 9679758]

Ernkvist M, Birot O, Sinha I, Veitonmaki N, Nystrom S, Aase K, Holmgren L. Differential roles of p80- and p130-angiomotin in the switch between migration and stabilization of endothelial cells. Biochim Biophys Acta. 2008; 1783:429–437. [PubMed: 18164266]

Ernkvist M, Luna Persson N, Audebert S, Lecine P, Sinha I, Liu M, Schlueter M, Horowitz A, Aase K, Weide T, et al. The Amot/Patj/Syx signaling complex spatially controls RhoA GTPase activity in migrating endothelial cells. Blood. 2009; 113:244–253. [PubMed: 18824598]

Forster C. Tight junctions and the modulation of barrier function in disease. Histochemistry and cell biology. 2008; 130:55–70. [PubMed: 18415116]

Furuta B, Harada A, Kobayashi Y, Takeuchi K, Kobayashi T, Umeda M. Identification and functional characterization of nadrin variants, a novel family of GTPase activating protein for rho GTPases. J Neurochem. 2002; 82:1018–1028. [PubMed: 12358749]

Giovannini M, Robanus-Maandag E, van der Valk M, Niwa-Kawakita M, Abramowski V, Goutebroze L, Woodruff JM, Berns A, Thomas G. Conditional biallelic Nf2 mutation in the mouse promotes manifestations of human neurofibromatosis type 2. Genes Dev. 2000; 14:1617–1630. [PubMed: 10887156]

Hanemann CO. Magic but treatable? Tumours due to loss of merlin. Brain. 2008; 131:606–615. [PubMed: 17940085]

Harada A, Furuta B, Takeuchi K, Itakura M, Takahashi M, Umeda M. Nadrin, a novel neuron-specific GTPase-activating protein involved in regulated exocytosis. J Biol Chem. 2000; 275:36885–36891. [PubMed: 10967100]

Hennigan RF, Foster LA, Chaiken MF, Mani T, Gomes MM, Herr AB, Ip W. Fluorescence resonance energy transfer analysis of merlin conformational changes. Mol Cell Biol. 2010; 30:54–67. [PubMed: 19884346]

Hirokawa Y, Tikoo A, Huynh J, Utermark T, Hanemann CO, Giovannini M, Xiao GH, Testa JR, Wood J, Maruta H. A clue to the therapy of neurofibromatosis type 2: NF2/merlin is a PAK1 inhibitor. Cancer J. 2004; 10:20–26. [PubMed: 15000491]

Iden S, Collard JG. Crosstalk between small GTPases and polarity proteins in cell polarization. Nat Rev Mol Cell Biol. 2008; 9:846–859. [PubMed: 18946474]

Jin H, Sperka T, Herrlich P, Morrison H. Tumorigenic transformation by CPI-17 through inhibition of a merlin phosphatase. Nature. 2006; 442:576–579. [PubMed: 16885985]

Kaempchen K, Mielke K, Utermark T, Langmesser S, Hanemann CO. Upregulation of the Rac1/JNK signaling pathway in primary human schwannoma cells. Hum Mol Genet. 2003; 12:1211–1221. [PubMed: 12761036]

Kalamarides M, Niwa-Kawakita M, Leblois H, Abramowski V, Perricaudet M, Janin A, Thomas G, Gutmann DH, Giovannini M. Nf2 gene inactivation in arachnoidal cells is rate-limiting for meningioma development in the mouse. Genes Dev. 2002; 16:1060–1065. [PubMed: 12000789]

Kissil JL, Johnson KC, Eckman MS, Jacks T. Merlin phosphorylation by p21-activated kinase 2 and effects of phosphorylation on merlin localization. J Biol Chem. 2002; 277:10394–10399. [PubMed: 11782491]

Kissil JL, Wilker EW, Johnson KC, Eckman MS, Yaffe MB, Jacks T. Merlin, the product of the Nf2 tumor suppressor gene, is an inhibitor of the p21-activated kinase, Pak1. Mol Cell. 2003; 12:841–849. [PubMed: 14580336]

Lallemand D, Curto M, Saotome I, Giovannini M, McClatchey AI. NF2 deficiency promotes tumorigenesis and metastasis by destabilizing adherens junctions. Genes Dev. 2003; 17:1090–1100. [PubMed: 12695331]

Lallemand D, Manent J, Couvelard A, Watilliaux A, Siena M, Chareyre F, Lampin A, Niwa-Kawakita M, Kalamarides M, Giovannini M. Merlin regulates transmembrane receptor accumulation and signaling at the plasma membrane in primary mouse Schwann cells and in human schwannomas. Oncogene. 2009; 28:854–865. [PubMed: 19029950]

Li W, You L, Cooper J, Schiavon G, Pepe-Caprio A, Zhou L, Ishii R, Giovannini M, Hanemann CO, Long SB, et al. Merlin/NF2 suppresses tumorigenesis by inhibiting the E3 ubiquitin ligase CRL4(DCAF1) in the nucleus. Cell. 2010; 140:477–490. [PubMed: 20178741]

Maitra S, Kulikauskas RM, Gavilan H, Fehon RG. The tumor suppressors Merlin and expanded function cooperatively to modulate receptor endocytosis and signaling. Curr Biol. 2006; 16:702–709. [PubMed: 16581517]

Miyoshi J, Takai Y. Molecular perspective on tight-junction assembly and epithelial polarity. Adv Drug Deliv Rev. 2005; 57:815–855. [PubMed: 15820555]

Morris ZS, McClatchey AI. Aberrant epithelial morphology and persistent epidermal growth factor receptor signaling in a mouse model of renal carcinoma. Proc Natl Acad Sci U S A. 2009; 106:9767–9772. [PubMed: 19487675]

Morrison H, Sperka T, Manent J, Giovannini M, Ponta H, Herrlich P. Merlin/neurofibromatosis type 2 suppresses growth by inhibiting the activation of Ras and Rac. Cancer Res. 2007; 67:520–527. [PubMed: 17234759]

Okada T, Lopez-Lago M, Giancotti FG. Merlin/NF-2 mediates contact inhibition of growth by suppressing recruitment of Rac to the plasma membrane. J Cell Biol. 2005; 171:361–371. [PubMed: 16247032]

Ramesh V. Merlin and the ERM proteins in Schwann cells, neurons and growth cones. Nat Rev Neurosci. 2004; 5:462–470. [PubMed: 15152196]

Richnau N, Aspenstrom P. Rich, a rho GTPase-activating protein domain-containing protein involved in signaling by Cdc42 and Rac1. J Biol Chem. 2001; 276:35060–35070. [PubMed: 11431473]

Rong R, Surace EI, Haipek CA, Gutmann DH, Ye K. Serine 518 phosphorylation modulates merlin intramolecular association and binding to critical effectors important for NF2 growth suppression. Oncogene. 2004; 23:8447–8454. [PubMed: 15378014]

Schulz A, Geissler KJ, Kumar S, Leichsenring G, Morrison H, Baader SL. Merlin inhibits neurite outgrowth in the CNS. J Neurosci. 2010; 30:10177–10186. [PubMed: 20668201]

Shaw RJ, Paez JG, Curto M, Yaktine A, Pruitt WM, Saotome I, O'Bryan JP, Gupta V, Ratner N, Der CJ, et al. The Nf2 tumor suppressor, merlin, functions in Rac-dependent signaling. Dev Cell. 2001; 1:63–72. [PubMed: 11703924]

Stokowski RP, Cox DR. Functional analysis of the neurofibromatosis type 2 protein by means of disease-causing point mutations. Am J Hum Genet. 2000; 66:873–891. [PubMed: 10712203]

Sugihara-Mizuno Y, Adachi M, Kobayashi Y, Hamazaki Y, Nishimura M, Imai T, Furuse M, Tsukita S. Molecular characterization of angiomotin/JEAP family proteins: interaction with MUPP1/Patj and their endogenous properties. Genes Cells. 2007; 12:473–486. [PubMed: 17397395]

Wells CD, Fawcett JP, Traweger A, Yamanaka Y, Goudreault M, Elder K, Kulkarni S, Gish G, Virag C, Lim C, et al. A Rich1/Amot complex regulates the Cdc42 GTPase and apical-polarity proteins in epithelial cells. Cell. 2006; 125:535–548. [PubMed: 16678097]

Wong HK, Lahdenranta J, Kamoun WS, Chan AW, McClatchey AI, Plotkin SR, Jain RK, di Tomaso E. Anti-vascular endothelial growth factor therapies as a novel therapeutic approach to treating neurofibromatosis-related tumors. Cancer Res. 2010; 70:3483–3493. [PubMed: 20406973]

Xiao GH, Beeser A, Chernoff J, Testa JR. p21-activated kinase links Rac/Cdc42 signaling to merlin. J Biol Chem. 2002; 277:883–886. [PubMed: 11719502]

Xiao GH, Gallagher R, Shetler J, Skele K, Altomare DA, Pestell RG, Jhanwar S, Testa JR. The NF2 tumor suppressor gene product, merlin, inhibits cell proliferation and cell cycle progression by repressing cyclin D1 expression. Mol Cell Biol. 2005; 25:2384–2394. [PubMed: 15743831]

Yi C, Kissil JL. Merlin in organ size control and tumorigenesis: Hippo versus EGFR? Genes Dev. 2010; 24:1673–1679. [PubMed: 20713513]

Yi C, Wilker EW, Yaffe MB, Stemmer-Rachamimov A, Kissil JL. Validation of the p21-activated kinases as targets for inhibition in neurofibromatosis type 2. Cancer Res. 2008; 68:7932–7937. [PubMed: 18829550]

Zhang N, Bai H, David KK, Dong J, Zheng Y, Cai J, Giovannini M, Liu P, Anders RA, Pan D. The Merlin/NF2 tumor suppressor functions through the YAP oncoprotein to regulate tissue homeostasis in mammals. Dev Cell. 2010; 19:27–38. [PubMed: 20643348]
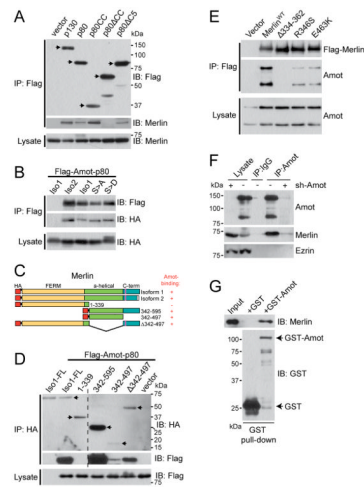
Figure 1. Merlin interacts with Angiomotin through their mutual CC domains

(A) Immunoblot (IB) analysis with Flag and Merlin antibodies of Flag Immunoprecipitates (IP) and total cell lysate from HEK293 cells transfected with various Flag-tagged Amot constructs as indicated.

(B) IB analysis with Flag and HA antibodies of Flag-IP and total cell lysate from HEK293 cells co-transfected with Flag-Amot-p80 and HA-tagged Merlin of either isoform (Iso1 or Iso2), or S518A (S>A) and S518D (S>D) mutants as indicated.

(C) Diagram of HA-tagged (represented by red bars) full-length Merlin and deletion constructs used in panel D below. S518 phosphorylation site is marked by a purple line. The N-terminal FERM domain is represented in yellow, the α-helical region in green, and the C-terminal domain (C-term) in blue. The Amot-binding status of each construct is indicated by "+" (binding) or "−" (no binding).

(D) IB analysis with HA and Flag antibodies of HA-IP and total cell lysate of HEK293 cells co-tranfected with Flag-Amot-p80 and various HA-tagged Merlin constructs as indicated. Hatched line indicates the merge of lanes from the same images of the same experiment/blot with an irrelevant intervening lane deleted.

(E) IB analysis with Merlin and Amot antibodies of Flag-IP and total cell lysate from HEK293 cells transfected with Flag-tagged wild-type (WT) or patient-derived mutant Merlin alleles as indicated.

(F) IB analysis with Amot, Merlin and Ezrin antibodies of total cell lysate or IP with Amot antibody or control IgG from HEK293 cells expressing control (−) or sh-Amot (+).

(G) IB analysis with Merlin and GST antibodies of GST pull-down of recombinant GST or GST-Amot-p80 proteins incubated with recombinant His-Merlin.
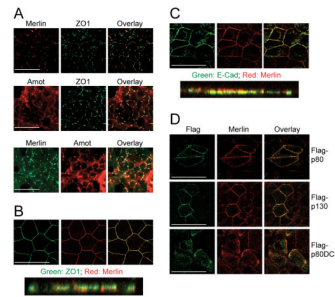
See also Figure S1.

Figure 2. Merlin co-localizes with Angiomotin to AJs and TJs in epithelial cells
(A) Immunofluorescence (IF) analysis of endogenous Merlin and ZO1 (upper panel), Amot and ZO1 (middle panel), or Merlin and Amot (lower panel) in HEK293 cells. Images were taken at 40X magnification.
(B and **C)** IF analysis of the endogenous localization of **(B)** Merlin (red) and ZO1 (green) or **(C)** Merlin (red) and E-Cad (green) in confluent MDCK cells. Confocal images (upper panels) were taken at 100X magnification. Deconvoluted Z-stacking images shown in lower panels.
(D) IF analysis of MDCK cells transfected with Flag-p80, Flag-p80ΔC5 or Flag-p130 with Flag and Merlin antibodies. Confocal images were taken at 100X magnification.
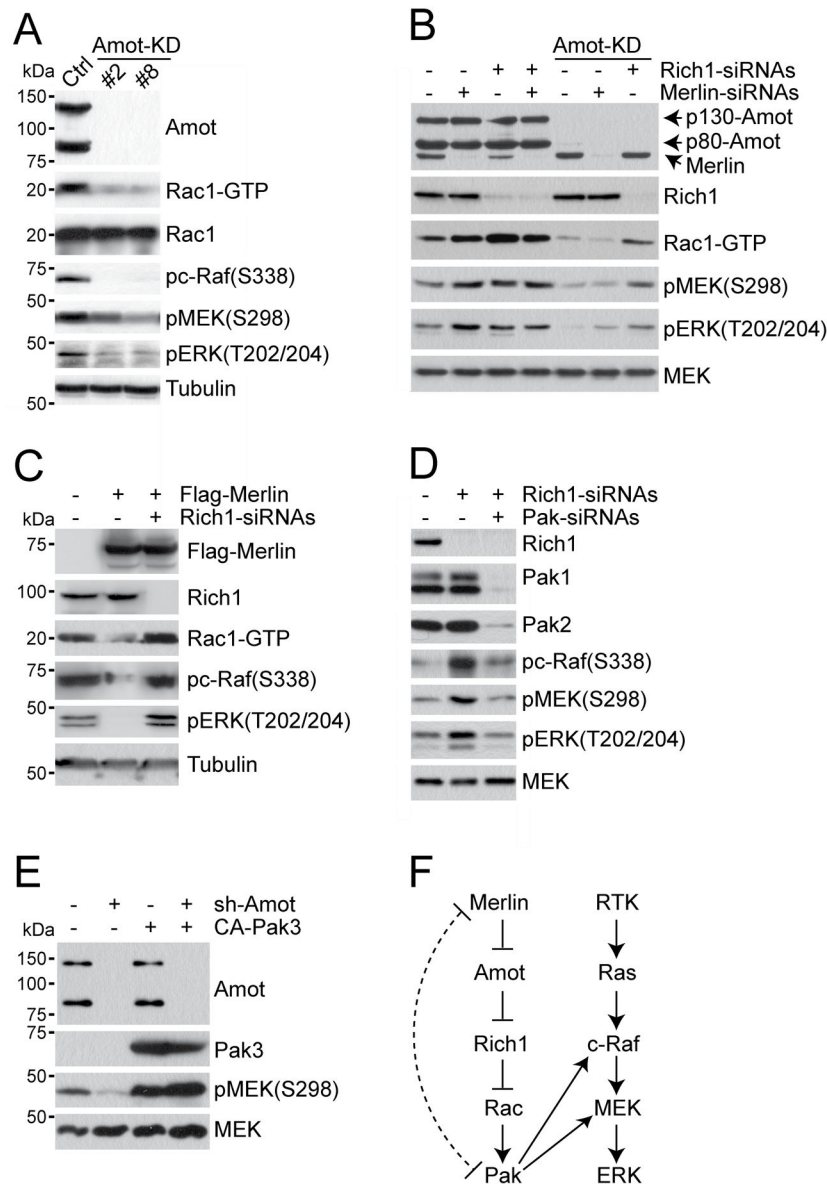Scale bars = 50 μm.
See also Figure S2.

Figure 3. Merlin functions through Angiomotin and Rich1 to inhibit Rac1 and Ras-MAPK signaling

(A) IB analysis of cell lysates from HEK293 cells stably expressing vector control (Ctrl) or two independent Angiomotin shRNAs (Amot-KD) with different antibodies as indicated. Tubulin used as internal loading control.

(B) IB analysis of cell lysate from HEK293 cells stably expressing vector control (Ctrl) or Angiomotin shRNAs (Amot-KD, clone #8) that were transfected with non-silencing control siRNAs (−) or siRNAs targeting Merlin or Rich1 (+). Total MEK protein used as internal loading control.

(C) IB analysis of cell lysate from HEK293 cells transiently transfected with Flag-Merlin with (+) or without (−) siRNAs targeting Rich1. Tubulin used as internal loading control.

(D) IB analysis of cell lysate from HEK293 cells transiently transfected with non-silencing control siRNAs (−) or siRNAs targeting Rich1 or Pak (+). Total MEK used as internal loading control.

(E) IB analysis of cell lysate from HEK293 cells stably expressing vector control (Ctrl) or Angiomotin shRNAs (Amot-KD, clone #8) that were transfected with empty vector (−) or constitutive-active form of Pak3 (+). Total MEK used as internal loading control. Cells were serum starved overnight and stimulated with 10 ng/mL EGF for 5′ in **(A-E)**. Data shown are representative of 3 independent experiments.

(F) Schematic representation of the Merlin-Angiomotin-Rich1-Rac1-Pak signaling cascade in relation to the Ras-ERK pathway. The dotted curved line reflects previous findings showing that Merlin can also directly inhibit Pak activity and in a negative feedback loop, Pak phosphorylates and inactivates Merlin.
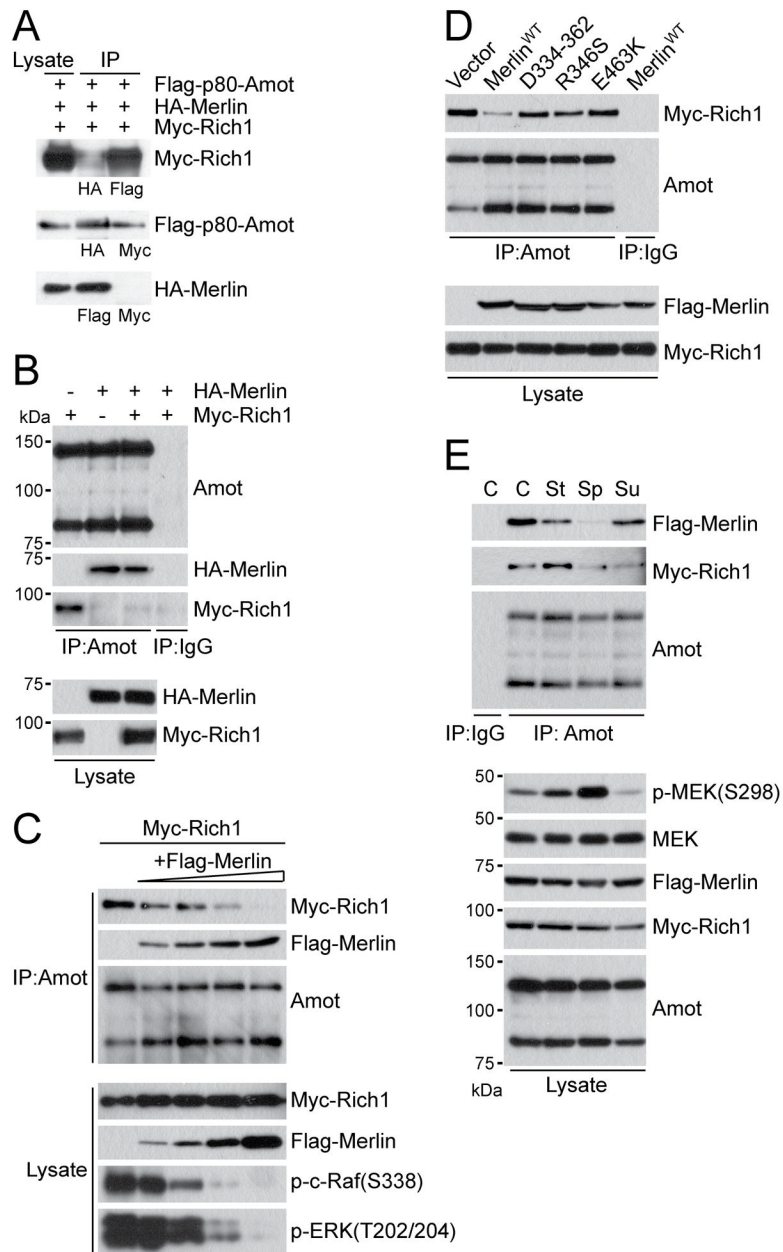
See also Figure S3.

Figure 4. Merlin competes with Rich1 for association with Angiomotin
(A) IP and IB analysis of cell lysates from HEK293 cells co-transfected with HA-Merlin, Flag-Amot-p80 and Myc-Rich1 with HA, Flag, or Myc antibodies as indicated.
(B) IB analysis of endogenous Angiomotin IP from HEK293 cells expressing equal amount of HA-Merlin and Myc-Rich1 alone or in combination. Normal rabbit IgG used as negative control.
(C) IB analysis of Myc-Rich1 and Flag-Merlin co-precipitated with endogenous Angiomotin or and total cell lysates from HEK293 cells expressing fixed amount of Myc-Rich1 (10μg) and incremental amount of Flag-Merlin (0, 1, 2.5, 5 and 10μg from left to right) with antibodies as indicated.
(D) IB analysis of Myc-Rich1 and Flag-Merlin co-precipitated with endogenous Angiomotin and total cell lysate from HEK293 cells expressing Myc-Rich1 alone or in combination with

Flag-tagged wild type or mutant Merlin alleles as indicated. Normal rabbit IgG used as negative control.

(E) IB analysis with indicated antibodies of Angiomotin IP and total cell lysate from HEK293 cells co-expressing Flag-Merlin and Myc-Rich1 under confluent (C), sparse (Sp), serum-stimulated (St), or suspension (Su) conditions. Normal rabbit IgG used as negative control. Total MEK used as internal loading control.
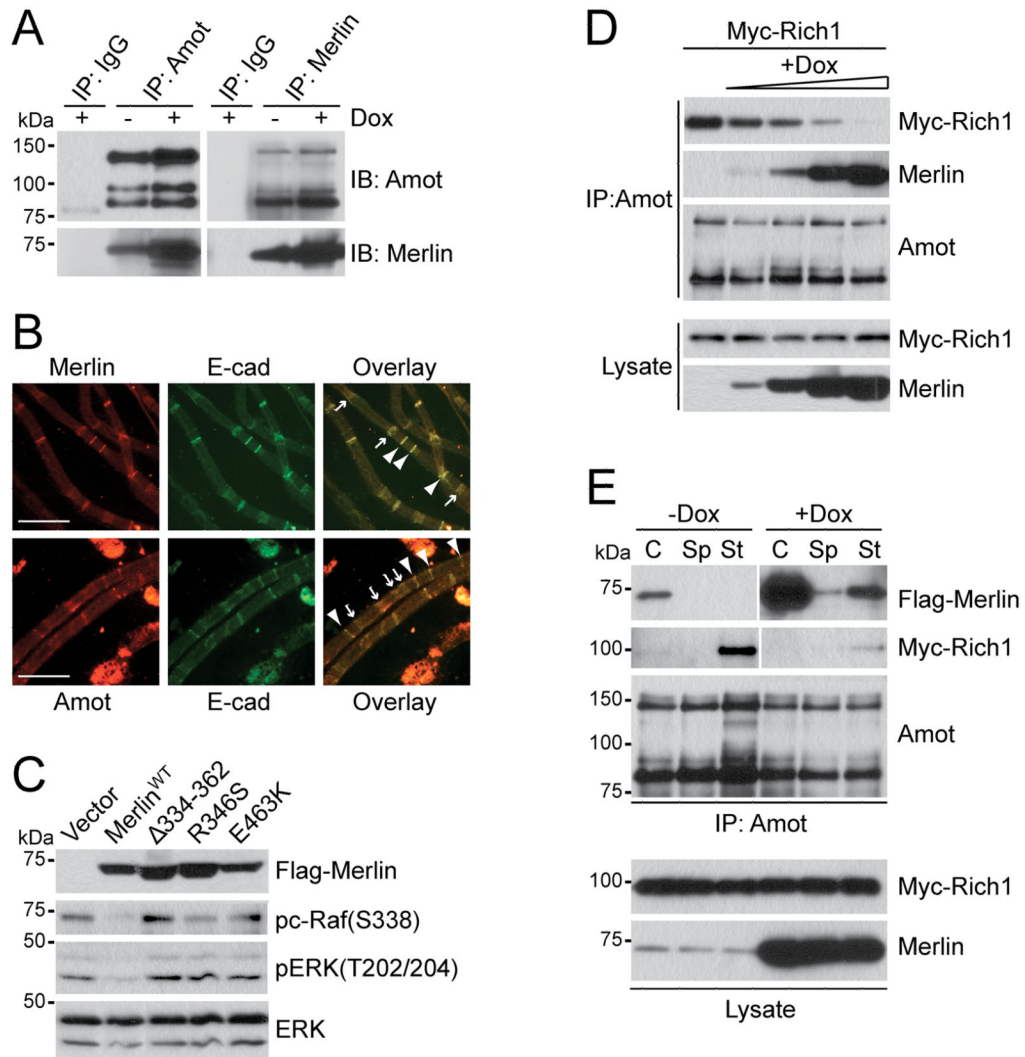
See also Figure S4.

Figure 5. Merlin interacts and co-localizes with Angiomotin in schwannoma cells and myelinating peripheral nerves

(A) IP and IB analysis with Amot or Merlin antibodies of cell lysates from untreated (−) or Doxycyline induced (+) RT4-67 cells as indicated.

(B) IF analysis of teased nerve fibers isolated from mouse sciatic nerves for Amot and E-cadherin (E-cad), or Merlin and E-cad as indicated. Arrowheads indicate the Schmidt-Lantermann incisures and paranodes. Images were taken at 40X magnification. Scale bar = 50 μm.

(C) IB analysis of Raf and ERK activation in cell lysates from RT4 cells transfected with vector control or Flag-tagged wild type or mutant Merlin as indicated.

(D) IB analysis of Myc-Rich1 and Merlin co-precipitated with endogenous Angiomotin and total cell lysates from RT4-67 cells expressing fixed amount of Myc-Rich1 (10μg) and treated with increasing dose of Doxycyline (0, 50, 100, 250 and 500 ng/ml from left to right) as indicated.

(E) IB analysis with indicated antibodies of Angiomotin IP or total cell lysate from untreated (−Dox) or Doxycyline induced (+Dox) RT4-67 transfected with Myc-Rich1 and grown under confluent (C), sparse (Sp), or serum-stimulated (St) conditions.
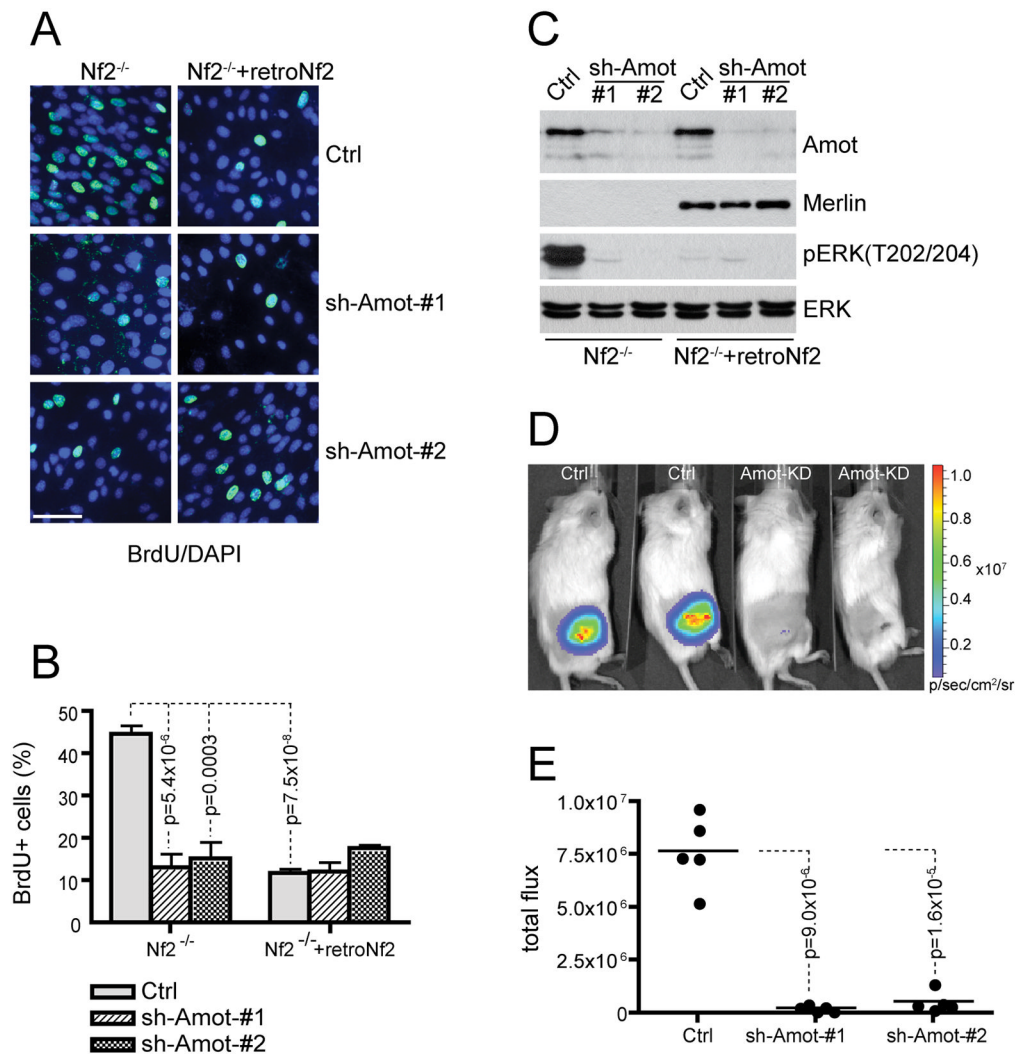See also Figure S4.

Figure 6. Angiomotin knockdown inhibits the proliferation and tumorigenicity of $Nf2^{-/-}$ Schwann cells

(A) Representative fields of BrdU (green) and DAPI (blue) double staining of $Nf2^{-/-}$ SC4 cells or Merlin-reconstituted SC4 cells ($Nf2^{-/-}$+retroNf2) infected with control (Ctrl) or Angiomotin shRNAs (sh-Amot #1 or #2). Cells were serum starved for 24 hours followed by incubation with BrdU in the presence of serum for 18 hours. Images were taken at 40X magnification. Scale bar = 50 μm.

(B) Quantitative analysis of the percentage of BrdU positive cells from **(A)**. Each bar represents the average percentage of BrdU$^+$ cells of 5 random fields from each cell line. Error bars indicate standard deviation (SD). p value was calculated with 2-tailed unpaired *Student's* t test.

(C) IB analysis of ERK activation in $Nf2^{-/-}$ SC4 cells or Merlin-reconstituted SC4 cells ($Nf2^{-/-}$+retroNf2) infected with control (Ctrl) or Angiomotin shRNAs (sh-Amot #1 or #2). Total ERK used as internal loading control.

(D) Representative images from bioluminescence imaging (BLI) of orthotopic tumors derived from control SC4/pLuc-mCherry cells (Ctrl) or Amot-KD SC4/pLuc-mCherry (Amot-KD) cells injected into sciatic nerve sheaths of NOD/SCID mice.

(E) Quantitative analysis of the total flux of luciferase signal from areas of injection. The sciatic nerves of three groups (N=5) of NOD/SCID mice were injected intraneurally with

2×10^5 Ctrl SC4/pLuc-mCherry or Amot-KD SC4/pLuc-mCherry cells (line #1 or line #2). All mice were imaged by BLI one week after the surgery. p value was calculated with 2-tailed unpaired *Student's* t test.
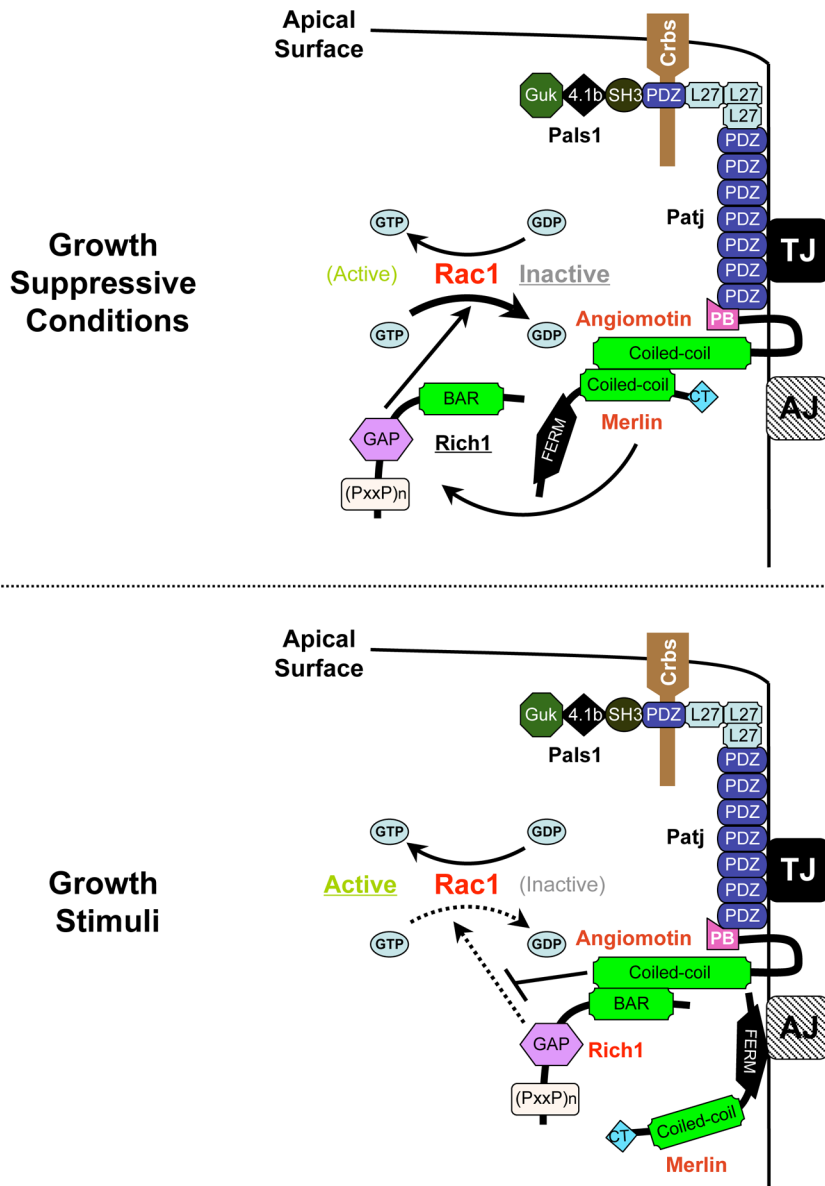
See also Figure S5.

Figure 7. Merlin inhibits Rac1 activity by releasing Rich1 from its TJ-associated inhibitor, Angiomotin

A model depicting the proposed mechanism of how the differential interactions between Merlin, Angiomotin and Rich1 modulate Rac1 activity. Under growth suppressive conditions, Merlin binds to Angiomotin, releasing Rich1 to inactivate Rac1 by converting Rac1-GTP to Rac1-GDP. In response to growth stimuli, Merlin dissociates from Angiomotin. Unoccupied Angiomotin binds to and blocks Rich1's GAP activity, leading to increased levels of Rac1-GTP.